Raman scattering of quasimodes in ZnO

2008 J. Phys.: Condens. Matter 20 445211

(http://iopscience.iop.org/0953-8984/20/44/445211)

J. Phys.: Condens. Matter **20** (2008) 445211 (4pp) doi:10.1088/0953-8984/20/44/445211

Raman scattering of quasimodes in ZnO

E Alarcón-Lladó[1], R Cuscó[1], L Artús[1], J Jiménez[2], B Wang[3] and M Callahan[4]

[1] Institut Jaume Almera, Consell Superior d'Investigacions Científiques (CSIC), Lluís Solé i Sabarís s.n., 08028 Barcelona, Spain
[2] Departamento de Física de la Materia Condensada, ETSII, Universidad de Valladolid, Spain
[3] Solid State Scientific Corporation, 27-2 Wright Road, Hollis, NH 03049, USA
[4] Air Force Research Laboratory, Sensors Directorate, Electromagnetics Technology Division, Optoelectronic Technology Branch, Hanscom AFB, MA 01731-2909, USA

Received 24 July 2008, in final form 19 September 2008
Published 10 October 2008
Online at stacks.iop.org/JPhysCM/20/445211

Abstract
The angular dependence of the optical phonons of high-quality bulk ZnO has been systematically studied by means of Raman scattering. We report the observation of quasi-TO and quasi-LO modes for propagation directions covering the whole a–c mixing plane using a beveled ZnO single crystal sample. Scattering experiments performed in two different configuration geometries indicate that birefringence effects are not relevant for the phonon analysis in this material. The observed angular dependence of the quasimode frequencies is in good agreement with Loudon's model.

1. Introduction

ZnO is a direct wide band-gap ($E_g \sim 3.4$ eV) semiconductor with a deep excitonic binding energy of around 60 meV [1], which makes it a promising material in electronics, optics and photonics. With reduction in size, semiconductor structures exhibit novel electronic, mechanical, optical and vibrational properties which are a consequence of surface and quantum confinement effects. Raman scattering has been proven to be a powerful and non-destructive technique to study the vibrational and optical properties of ZnO crystals, thin films and micro and nanostructures [2–4]. In the case of crystals of reduced dimensionality, some peak shifts and broadenings in the Raman spectra may occur. In previous works on ZnO nanocrystals, some authors attribute these changes to confinement effects [5–9], whereas others claim that the shifts are due to local heating rather than to spatial confinement [10, 11]. However, the crystallite orientation also affects the Raman spectra. In these systems, a mixing of the polar modes takes place when the crystal high-symmetry axes are tilted relative to the phonon propagation direction. This gives rise to the so-called quasimodes [12] and their frequency changes depending on the light incidence. Ignoring the excitation of quasimodes in nanostructures could result in a misleading analysis of strain, composition and confinement.

Some works dealing with quasimodes in wide band-gap materials have been published [13–16]. Bergman *et al* [13] studied the quasi-transverse and quasi-longitudinal optical modes in wurtzite AlN for phonon propagation angles lower than 30° relative to the a-axis. Early works on quasimodes in ZnO were performed in the late 1960s, but only showed spectra for a 45° phonon propagation direction [15, 16]. To date, no Raman data on the angular dependence of quasimodes in ZnO are available. In this work we present a systematic study of the longitudinal optical (LO) and transverse optical (TO) quasimodes in bulk single crystal ZnO by means of Raman scattering for phonon propagation angles spanning the whole range of propagation directions between the a and c axis. We discuss the role of birefringence in the determination of the quasimode frequencies in wurtzite crystals and we find that the birefringence effects can be neglected in ZnO. The experimental values of the quasimode frequencies are in good agreement with those predicted by Loudon's model based on the phonon–electrostatic field interaction between polar modes in uniaxial materials.

2. Experiment

The experiments were performed on a ZnO single crystal obtained by the hydrothermal growth method. Growth details as well as x-ray and photoluminescence (PL) characterization of ZnO crystals obtained by this growth method can be found elsewhere [17]. The sample was excited at room temperature with the 514.5 nm line of an Ar^+ laser in the backscattering geometry from an m-plane ($10\bar{1}0$). The scattered light was analyzed with a Jobin-Yvon T64000 spectrometer equipped with a LN_2-cooled charged-coupled device (CCD) detector.

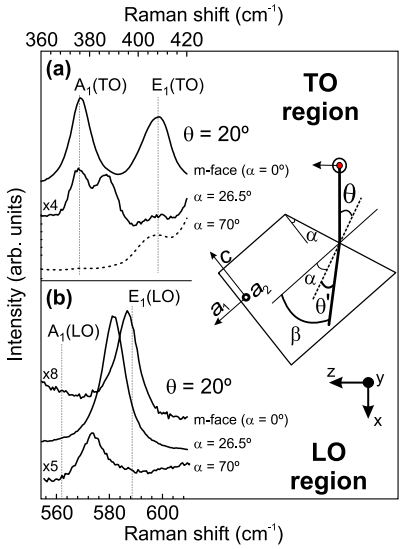

Figure 1. Room temperature $x(z\gamma)\bar{x}$ Raman spectra of single crystal ZnO in the TO (a) and LO (b) frequency regions. The spectra were obtained with an angle of incidence of 20° from various surfaces. The dotted spectrum was recorded in a $x(y\gamma)\bar{x}$ configuration in order to reduce the E_2^{high} tail. The spectra are arbitrarily offset on the intensity scale for clarity. The sketch shows the geometry of the experimental setup and the laboratory coordinate system (x, y, z). θ, θ' and α correspond to the incidence, refracted and surface tilting angles, respectively, and $\beta = \alpha + \theta'$.

Both $x(z\gamma)\bar{x}$ and $x(y\gamma)\bar{x}$ scattering configurations were used, where x, y, and z correspond to the laboratory coordinates as depicted in figure 1, and γ denotes the scattered light polarization which depends on the angle θ and was adjusted by optimizing the quasimode signal. We define a set of orthogonal crystal axes (a_1, a_2, c), where a_1 (a_2) is perpendicular (parallel) to the m-plane and c is along the (0001) crystallographic direction (see sketch in figure 1). The ZnO crystal was rotated in 10° steps through an angle θ in such a way that the quasiphonon propagation direction remains in the mixing c–a_1 plane. In the backscattering geometry, the phonon propagation direction lies along the light propagation direction in the crystal. The maximum phonon propagation angle β is thus limited to around 30° in ZnO by Snell's law. In order to overcome this limitation and to attain higher phonon propagation angles, we also performed measurements on surfaces tilted at an angle $\alpha = 26.5°$ and 70° relative to the m-plane. The former corresponds to the natural growth surface $(10\bar{1}1)$, whereas for the latter a beveled sample was prepared by chemomechanical polishing at NovaSiC.

3. Results and discussion

Figure 1 shows $x(z\gamma)\bar{x}$ Raman spectra performed at an incidence of $\theta = 20°$ relative to the surface normal, for surfaces tilted at an angle $\alpha = 0$, 26.5, and 70°, where β increases from ≈10° for $\alpha = 0°$ to ≈80° for $\alpha = 70°$. In the TO-frequency region (figure 1(a)), three main features can be observed in the spectra: the E_1(TO) mode at 407.1 cm^{-1}, the A_1(TO) mode at 374.7 cm^{-1}, and a peak which shifts upwards with increasing β. In the LO-frequency region (figure 1(b)), a single intense peak dominates the spectrum. This peak shifts to lower frequencies as the propagation angle increases. Given that in ZnO the interaction between polar modes is dominated by the long-range electrostatic field rather than by the short-range interatomic forces, TO (LO) phonons of A_1 and E_1 symmetries mix together, giving rise to quasimodes with large TO–LO splitting. These quasimodes exhibit nearly pure transverse (quasi-TO) or longitudinal (quasi-LO) character and their frequencies shift relative to the frequencies of the pure modes depending on the phonon propagation direction [12]. Therefore we assign the peaks displaying a frequency dependence on the propagation angle in figures 1(a) and (b) to the quasi-TO and quasi-LO modes, respectively. The E_1 character of the quasi-TO mode increases with the phonon propagation angle and therefore it displays a shift to higher frequencies. Conversely, the quasi-LO mode gains A_1 character as the phonon propagation angle increases and as a result it shows a downward frequency shift.

For incidences close to the c-axis the weak quasi-TO mode cannot be well resolved because it is masked by the overlapping E_2^{high} low frequency tail. For this reason, we plot in figure 1(a) the $x(y\gamma)\bar{x}$ spectrum for $\alpha = 70°$ (dotted line). In contrast, the quasi-LO mode intensity becomes comparable with that of the typical second order Raman features in ZnO [2] but can still be unambiguously determined.

As already mentioned, pure E_1(TO) and A_1(TO) peaks show up in the spectra (see figure 1(a)) in spite of the mixing between the A_1 and E_1 modes. The pure E_1(TO) mode observed in the $x(z\gamma)\bar{x}$ Raman spectra corresponds to the E_1 component polarized along the direction orthogonal to the c–a_1 mixing plane. Although the non-degenerate A_1 mode lies in the c–a_1 plane and always mixes with the E_1 mode, a weak pure A_1(TO) mode is also observed in the $x(z\gamma)\bar{x}$ spectra which is attributed to Raman scattering of internal reflections.

In order to collect and show all our experimental data, we present in figure 2 a contour plot of the Raman intensity over the range of incidence and surface tilting angles studied in this work. For convenience, the x-axis range is arranged so that no discontinuities in the phonon propagation angle occur between plots from differently tilted surfaces. The intensity was normalized to the quasimode intensity after a baseline subtraction and the maxima and minima of intensity correspond, respectively, to the red and blue colors in the contour plot. First, we note that both the quasi-TO and the quasi-LO modes do not show a significant variation of their width with the incidence and surface tilting angles. However, the quasi-TO mode seems to broaden asymmetrically to lower frequencies with increasing θ in the $\alpha = 26.5°$ lower panel of figure 2. This broadening can be explained by the presence of a weak pure A_1(TO) mode superimposed to the quasimode whose origin has been discussed above. For $\alpha = 70°$ the quasi-TO mode weakens and shifts upward, allowing the pure A_1(TO) be clearly observed in the contour plot as an independent peak (dark region in the lower right panel). The fact that quasimodes display similar widths for all propagation directions is not surprising, as the A_1 and E_1-symmetry modes have similar widths in ZnO either for the longitudinal and

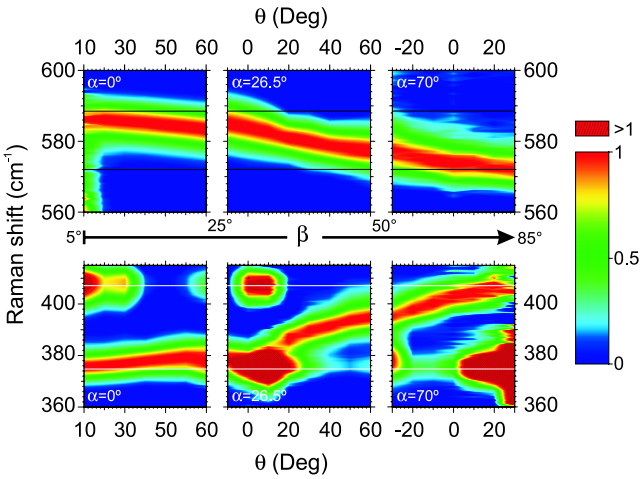

Figure 2. Spectrally resolved contour plots of the $x(z\gamma)\bar{x}$ Raman intensity as a function of the angle of incidence in the LO-frequency region (upper panels) and TO-frequency region (lower panels). Spectra were taken from faces tilted an angle α relative to the m-face. The arrow indicates increasing phonon propagation angle. The spectra were normalized such that the quasimode intensity is unity. Horizontal lines represent the frequency position of the pure polar modes in ZnO.

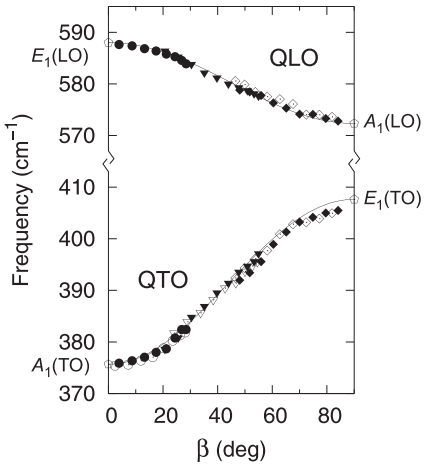

Figure 3. Quasi-LO and quasi-TO mode frequencies as a function of phonon propagation angle β relative to the a_1 axis. The plotted data points were obtained from a m-face (circles) and faces tilted 26.5° (triangles) and 70° (diamonds). Empty (filled) symbols correspond to the $x(y\gamma)\bar{x}$ [$x(z\gamma)\bar{x}$] scattering configuration. Solid lines represent the quasimode frequencies calculated using Loudon's theory.

transverse modes [2]. On the other hand, the quasimode frequency behavior is clearly illustrated in figure 2. The quasi-LO mode frequency ω_{QLO} (upper panels) shifts monotonically from the E_1(LO) mode frequency, $\omega_{E_1(\mathrm{LO})} = 588.5\ \mathrm{cm}^{-1}$, to the A_1(LO) mode frequency, $\omega_{A_1(\mathrm{LO})} = 571.0\ \mathrm{cm}^{-1}$, when changing the phonon propagation direction from a_1 to c. A similar behavior holds for the quasi-TO mode frequency. The mode shows an upward frequency shift from the A_1(TO) to the E_1(TO) mode frequency ($\omega_{A_1(\mathrm{TO})} = 378.0\ \mathrm{cm}^{-1}$ and $\omega_{E_1(\mathrm{TO})} = 410.0\ \mathrm{cm}^{-1}$, respectively). As the longitudinal mode frequencies are closer to each other than the transverse mode frequencies, the dispersion of the quasi-TO mode ($\sim$32 cm^{-1}) is larger than that of the quasi-LO mode ($\sim$16 cm^{-1}).

The change of the quasimode frequency with β can be modeled by Loudon's theory, considering the long-range electrostatic field as the dominant interaction mechanism between polar phonons. Under this assumption, the theory predicts that the quasi-TO mode frequency should lie between the frequency of the pure A_1(TO) mode and that of the pure E_1(TO) mode according to the relation [12]

$$\omega^2_{\mathrm{QTO}} = \omega^2_{A_1(\mathrm{TO})}\cos^2\beta + \omega^2_{E_1(\mathrm{TO})}\sin^2\beta. \qquad (1)$$

Similarly, the quasi-LO mode should shift from the pure E_1(LO) mode to the pure A_1(LO) mode following the relation [12]

$$\omega^2_{\mathrm{QLO}} = \omega^2_{E_1(\mathrm{LO})}\cos^2\beta + \omega^2_{A_1(\mathrm{LO})}\sin^2\beta. \qquad (2)$$

In the backscattering geometry, β can be derived from the incidence angle θ and the surface tilting angle α via Snell's law: $n_1\sin\theta = n_2\sin(\beta-\alpha)$, where $n_1 = 1$ and n_2 is the ZnO refractive index. As ZnO is a uniaxial crystal, two different refractive indices are to be considered depending on the electric field direction of the incident light. For the electric field parallel (perpendicular) to the c-axis, the extraordinary refractive index n_e (ordinary refractive index n_o) must be used. In the $x(z\gamma)\bar{x}$ configuration geometry, the refractive index varies from n_e for normal incidence to n_o in the $\beta \to 90°$ limit according to the refractive index ellipsoid $1/n^2(\beta) = (\sin\beta/n_o)^2 + (\cos\beta/n_e)^2$. In contrast, in a $x(y\gamma)\bar{x}$ configuration geometry the refractive index is n_o independently of the angle of incidence θ. However, for small β only the quasi-TO mode can be unambiguously detected in this configuration. For this reason, experiments in the two scattering configurations discussed above were carried out.

Figure 3 displays the experimental values of ω_{QTO} and ω_{QLO} as a function of the phonon propagation angle β. The angle β was calculated using $n_2 = n_o = 2.053$ [18] as the refractive index of ZnO for both scattering geometries used in the experiments. If birefringence effects were important, the two sets of data plotted in figure 3 would differ noticeably. On the contrary, a smooth overlapping of the experimental data can be seen in figure 3, from which we conclude that the error made by using the approximation $n(\beta) = n_o$ is negligible and therefore birefringence effects can be ignored in ZnO for the purpose of quasimode analysis. The experimental quasimode frequencies follow closely the theoretical predictions (equations (1) and (2)), also plotted in figure 3 as solid lines. Although at large β the quasi-TO mode frequencies deviate slightly from the theoretical curve, this may be related to the difficulty in determining accurately ω_{QTO} in this limit, given the high intensity of the E_2^{high} peak whose low frequency tail overlaps the weak quasi-TO mode.

4. Conclusions

The quasi-LO and quasi-TO modes of ZnO were observed for the whole range of phonon propagation angles between an a and the c axis. The angular dependence of the

quasimode frequencies is well described by Loudon's model. The agreement between the model and the experimental data obtained under different scattering geometries implies that the birefringence effect can be neglected in ZnO for the phonon analysis. Taking into account this angular dependence is crucial for analyzing Raman spectra of nanostructured ZnO with randomly oriented facets.

Acknowledgments

Work supported by the Spanish Government (project MAT2007-63617 and FPI Program). The work performed by the US Air Force Research Laboratory at Hanscom Air Force Base was partially supported by the Air Force Office of Scientific Research.

References

[1] Thomas D 1960 *J. Phys. Chem. Solids* **15** 86
[2] Cuscó R, Alarcón-Lladó R, Ibáñez J, Artús L, Jiménez J, Wang B and Callahan M 2007 *Phys. Rev.* B **75** 165202
[3] Park D, Tak Y and Yong K 2008 *J. Nanosci. Nanotechnol.* **8** 623
[4] Chen B, HT N and Chen C L 2007 *J. Exp. Nanosci.* **2** 57
[5] Bergman L, Chen X B, Huso J, Morrison J L and Hoeck H 2005 *J. Appl. Phys.* **98** 093507
[6] Zi J, Büscher H, Falter C, Ludwig W, Zhang K and Xie X 1996 *Appl. Phys. Lett.* **69** 200
[7] Campbell I H and Fauchet P M 1986 *Solid State Commun.* **58** 739
[8] Rajalakshmi M, Arora A K, Bendre B S and Mahamuni S 2000 *J. Appl. Phys.* **87** 2445
[9] Geng C, Jiang Y, Yao Y, Meng X, Zapien J A, Lee C S, Lifshitz Y and Lee S T 2004 *Adv. Funct. Mater.* **14** 589
[10] Alim K A, Fonoberov V A, Shamsa M and Balandin A A 2005 *J. Appl. Phys.* **97** 124313
[11] Demangeot F, Paillard V, Chassaing P M, Pagès C, Kahn M L, Maisonnat A and Chaudret B 2006 *Appl. Phys. Lett.* **88** 071921
[12] Loudon R 1964 *Adv. Phys.* **13** 423
[13] Bergman L, Dutta M, Balkas C, Davis R F, Christman J A, Alexson D and Nemanich R J 1999 *J. Appl. Phys.* **85** 3535
[14] Filippidis L, Siegle H, Hoffmann A, Thomsen C, Karch K and Bechstedt F 1996 *Phys. Status Solidi* b **198** 621
[15] Arguello C A, Rousseau D L and Porto S P S 1969 *Phys. Rev.* **181** 1351
[16] Damen T C, Porto S P S and Tell B 1966 *Phys. Rev.* **142** 570
[17] Suscavage M, Harris M, Bliss D, Yip P, Wang S Q, Schwall D, Bouthillette L, Bailey J, Callahan M and Look D C 1999 *MRS Internet J. Nitride Semicond. Res.* **4S1** G3.40
[18] Yoshikawa H and Adachi S 1997 *Japan J. Appl. Phys.* **36** 6237